Int. J. Multiphase Flow Vol. 19, No. 5, pp. 751–763, 1993
Printed in Great Britain.

0301-9322/93 $6.00 + 0.00

GAS–LIQUID FLOW PATTERNS AT MICROGRAVITY CONDITIONS

L. ZHAO and K. S. REZKALLAH
Department of Mechanical Engineering, University of Saskatchewan, Saskatoon, Canada S7N 0W0

(Received 24 August 1992; in revised form 25 May 1993)

Abstract—Understanding two-phase flow at microgravity conditons is important to a variety of space applications, including the design of thermal transport systems for the anticipated high-power-level space station. Two-phase air–water flow pattern data are reported at microgravity conditions during a series of parabolic trajectories flown on the NASA KC-135 aircraft. The liquid superficial velocity ranges from 0.09 to 3.73 m/s, and the gas superficial velocity from 0.2 to 29.9 m/s. Bubble, slug, frothy slug–annular and annular flows are observed to exist. Transitions between the different flow patterns are analyzed based on a force balance approach. It is found that the gas-phase Weber number serves as an excellent criterion for the transitions from slug to frothy slug–annular flows, and also from frothy slug–annular to annular flows.

Key Words: two-phase flow, flow patterns, microgravity

INTRODUCTION

Gas–liquid flow at microgravity (μ-g) conditions has been a subject of considerable research over the past 10 years, and has continuously drawn attention from researchers all over the world. Mainly due to the requirement for the design and operation of an active two-phase thermal transport system (known as a "thermal bus") for the anticipated high-power-level space station, the flow patterns, pressure drops and heat transfer coefficients of two-phase flow at μ-g conditions must be evaluated. As the gravity level is reduced, the mechanics of the flow are expected to change as a result of a new balance between the different forces acting on the fluids. The pressure drop and heat transfer coefficient are expected to be different from those at normal gravity conditions.

A pioneer work on μ-g gas–liquid flow was presented by Heppner *et al.* (1975). Experiments were performed at reduced-gravity aboard the NASA KC-135 aircraft using a water–air system with a 2.54 cm dia tube having an L/D ratio of about 20. The pressure-drop data and flow pattern observations indicated that the behavior of two-phase systems at low gravity would differ from that at 1-g. Flow patterns were classified as segregated, intermittent and distributed. The boundaries between the flow patterns at μ-g are different from those at 1-g.

Flow pattern observations were also made during a series of Learjet flights and also in the NASA Lewis 30 m drop tower, and were reported by Dukler *et al.* (1988). Experiments were carried out using water–air in a 0.95 cm i.d. tube ($L = 46$ cm, $L/D = 48$) at the NASA Lewis 30 m drop tower facility, which provided about 2.2 s of near-zero gravity. The Learjet test loop had a test section of 1.27 cm i.d. and a 106 cm long tube. Each parabolic trajectory provided 12–22 s of near-zero gravity test time. Flow visualization was obtained using a high-speed camera (400 fps), and it seems that the camera was placed about 80 cm from the inlet ($L/D \approx 63$). Data were selected when the acceleration did not exceed $0.02\,g_0$, where g_0 is the gravity at ground level. Flow visualization showed that the local relative velocity between the liquid and gas is negligible for bubble and slug flows. A model was suggested to predict the transitions between bubble and slug flows, as well as between slug and annular flows. However, surface-tension effects, which are important at μ-g conditions, were not considered.

Colin *et al.* (1991) conducted an experiment during a series of parabolic trajectories that provided 15–20 s of reduced gravity at levels $< 0.03\,g_0$. The test section was 4 cm i.d. and 200 cm long ($L/D = 50$). Flow patterns at the inlet and outlet of the test section were videotaped on high-speed television equipment operating at 500 fps. Void fraction, pressure drop and flow pattern observations were recorded during those tests. The pressure-drop measurements suggested that the wall

Table 1. Summary of previous experimental test conditions

Authors	Facility	Fluids	L/D	i.d. cm
Heppner *et al.* (1975)	Aircraft	Water–air	20	2.54
Dukler *et al.* (1988)	Aircraft	Water–air	63	0.95
Colin *et al.* (1991)	Aircraft	Water–air	50	4.0
Huckerby & Rezkallah (1992 a,b)	Aircraft	Water–air	84	0.95

friction can be reasonably estimated using the homogeneous model at 1-g. Measurements of the bubble size distribution at the inlet and outlet locations of the test section showed that there was a high rate of coalescence as the mixture flows downstream.

More recently, Huckerby & Rezkallah (1992 a,b) performed several gas–liquid flow experiments on the NASA KC-135 test aircraft. The observation section was 9.525 mm i.d. and 80 cm long. Flow patterns were recorded on a Hi-8 mm videocamera. In those studies, the liquid superficial velocity ranged from 0.075 to 3.81 m/s, and the gas superficial velocity from 0.1 to 29.9 m/s. Bubble, slug and annular flows were reported to exist. Their data broadened the data bank of gas–liquid flow at μ-g conditions. Table 1 briefly summarizes the test conditions used in all the previous experiments.

On the other hand, theoretical studies were performed in order to extend the avaliable correlations for transitions between different flow patterns for the 1-g maps to μ-g. Karri & Mathur (1988) extrapolated the 1-g models of Taitel *et al.* (1980), Taitel & Dukler (1976) and Weisman *et al.* (1979) for horizontal and vertical flows to μ-g conditions. In general, this method was not successful when compared against the existing μ-g data (Rezkallah 1990; Huckerby & Rezkallah 1992a).

Lee *et al.* (1987) developed a theoretical μ-g two-phase flow pattern map. The flow patterns considered were annular flow, dispersed flow, slug flow and stratified flow. A force balance including body forces, surface-tension forces, inertial forces, friction and the force due to eddy turbulent fluctuations was presented. Stratified flow was assumed to occur when the body forces

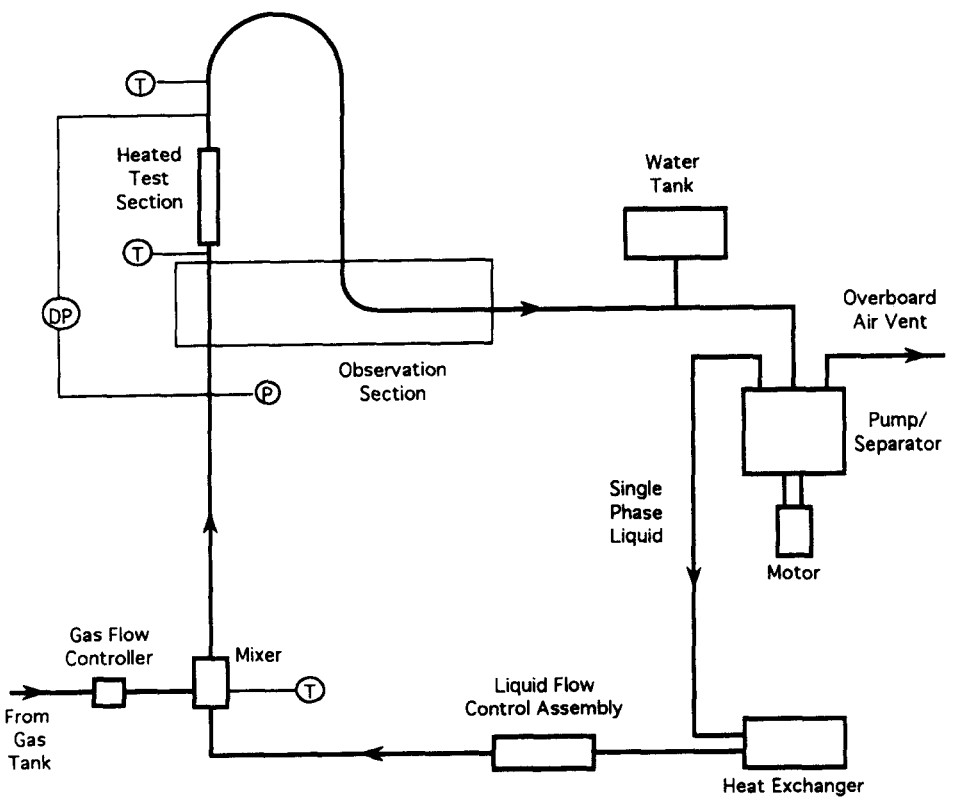

Figure 1. A schematic diagram of the test facility.

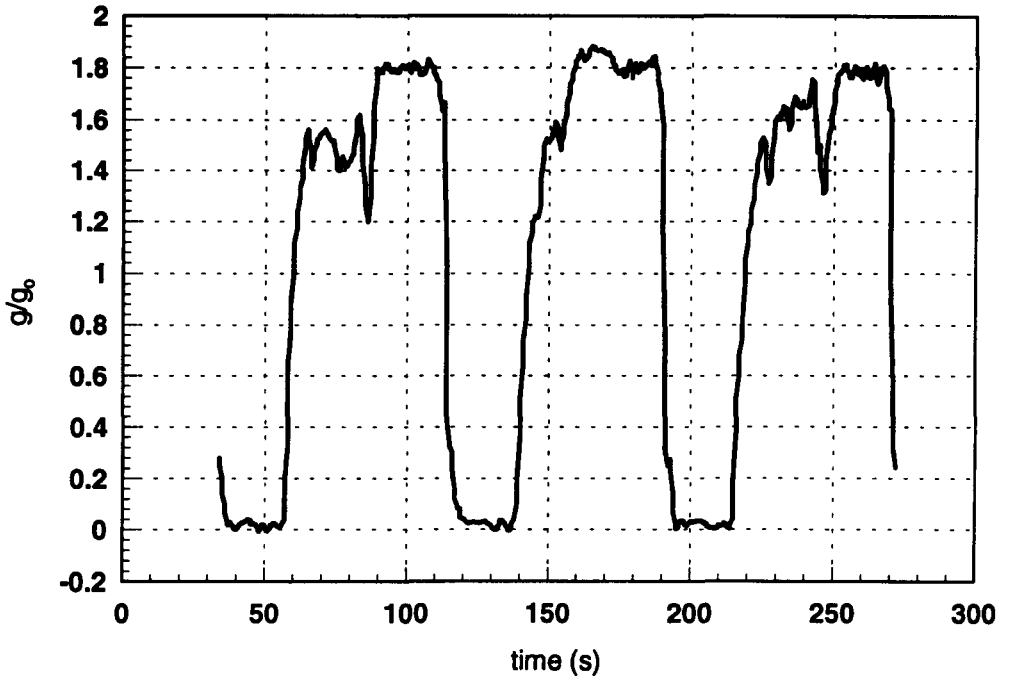

Figure 2. Gravity change as a function of time during typical KC-135 parabolas.

are larger than the surface-tension forces; while the transition from slug flow to dispersed bubbly flow would take place when the force from turbulent fluctuations is greater than the surface-tension force. Lastly, the transition from slug to annular flow was argued to take place when the force due to gas inertia is larger than that due to surface tension.

Rezkallah *et al.* (1990) performed an analysis to examine the forces acting on gas–liquid forced-convective flow under 1-g and microgravity conditions. The analysis was performed using simplified models for the bubble and slug flow patterns. A summary of the research work on two-phase flow patterns at μ-g conditions up to 1987 was given by Rezkallah (1990).

In the present study, air–water two-phase flow pattern data at μ-g conditions are presented. Transitions between the different flow patterns are analyzed based on a balance between the different forces acting on the flow. A simple criterion is proposed for the flow pattern transition boundaries. Also, the present model is compared with other experimental data available in the open literature.

EXPERIMENTAL APPARATUS

The test facility, shown schematically in figure 1, was used for the μ-g experiments on the NASA KC-135 aircraft. The test apparatus consists of a test section, a liquid-flow loop, a gas-flow loop, a pump/separator unit, a mixer, a data acquisition system and flow pattern recording cameras.

The two phases were supplied through a mixer. The mixer was designed such that the gas enters the mixer from several small holes in the wall, and is mixed with the liquid which flows axially in the mixing chamber. Prior to the test section, the mixture passed through a 80 cm long calming length (0.9525 cm i.d.). The test section consists of five parts: a vertical upward observation section (12.7 cm long, 0.9525 cm i.d.); a vertical upward heated test section (36 cm long, 0.9525 cm i.d.); a vertical downward observation section (58.4 cm long, 1.27 cm i.d.); a 90° bend observation section (7.65 cm radius, 1.27 cm i.d.); and a horizontal observation section (39.4 cm long, 1.27 cm i.d.). The observation sections were set into a "light-path-corrector" to reduce distortion near the wall due to the curvature of the tube. The light-path-corrector is an acrylic box filled with glycol, which has nearly the same index of refraction as the acrylic tube. Only the flow observations at the vertical upward test section are reported and discussed in this paper.

Water and air were used as working fluids. Water was pumped in a closed loop from the

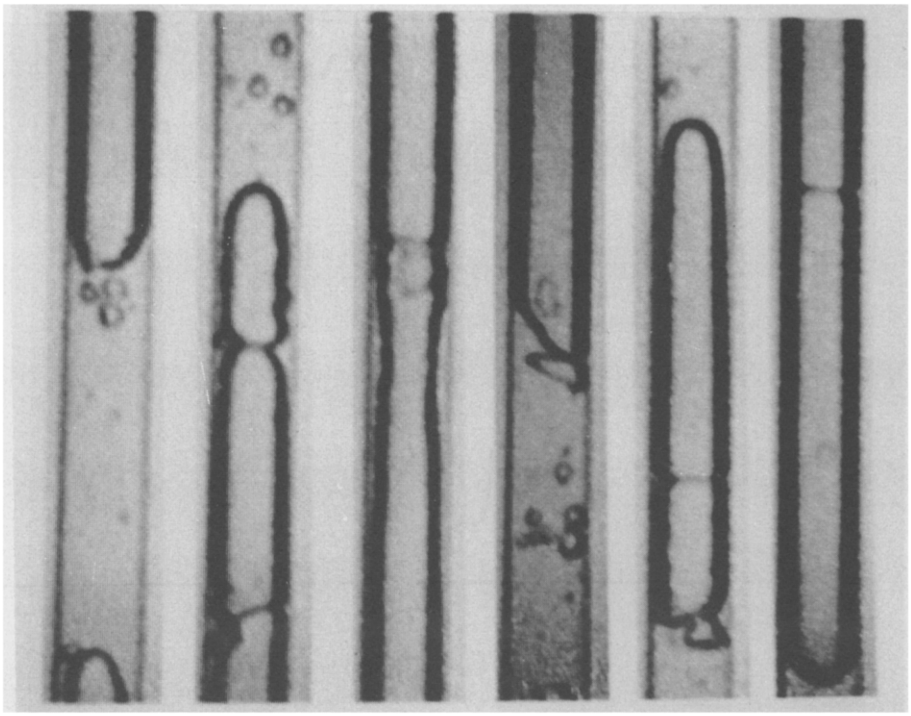

Figure 3. μ-g Flow patterns at $V_{SL} = 0.2$ m/s and $V_{SG} = 0.11$ m/s.

pump/separator unit through the experimental section and back to the pump/separator. The water flow rate was varied by adjusting the rotational speed of the pump, and also through the flow control valve, and was measured using a turbine meter with an accuracy of 0.5%. Air was supplied from a compressed air tank attached to the apparatus. It was regulated from the tank pressure of

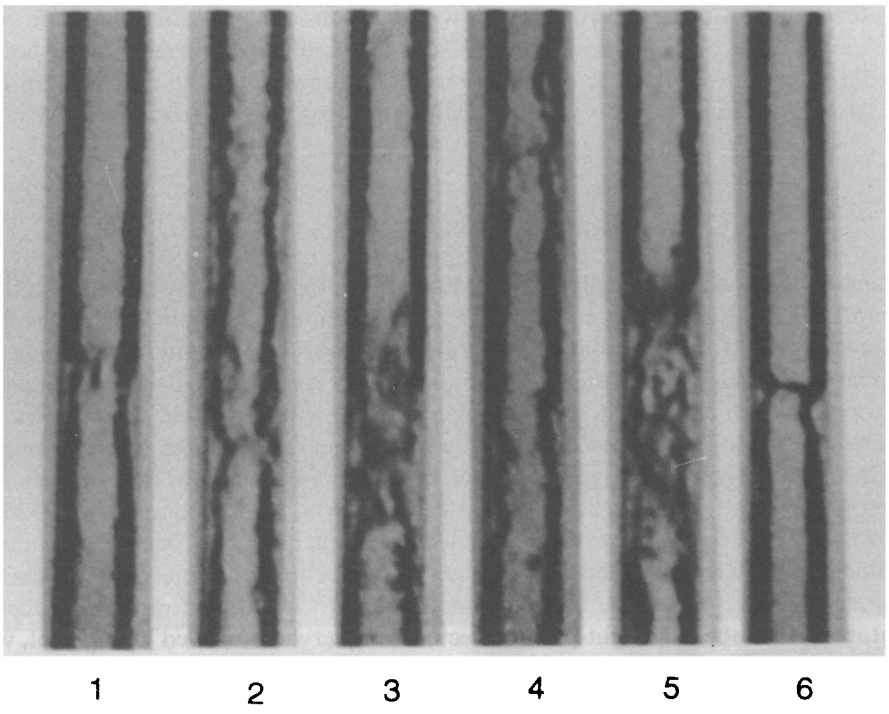

Figure 4. μ-g Flow patterns at $V_{SL} = 0.2$ m/s and $V_{SG} = 6.97$ m/s.

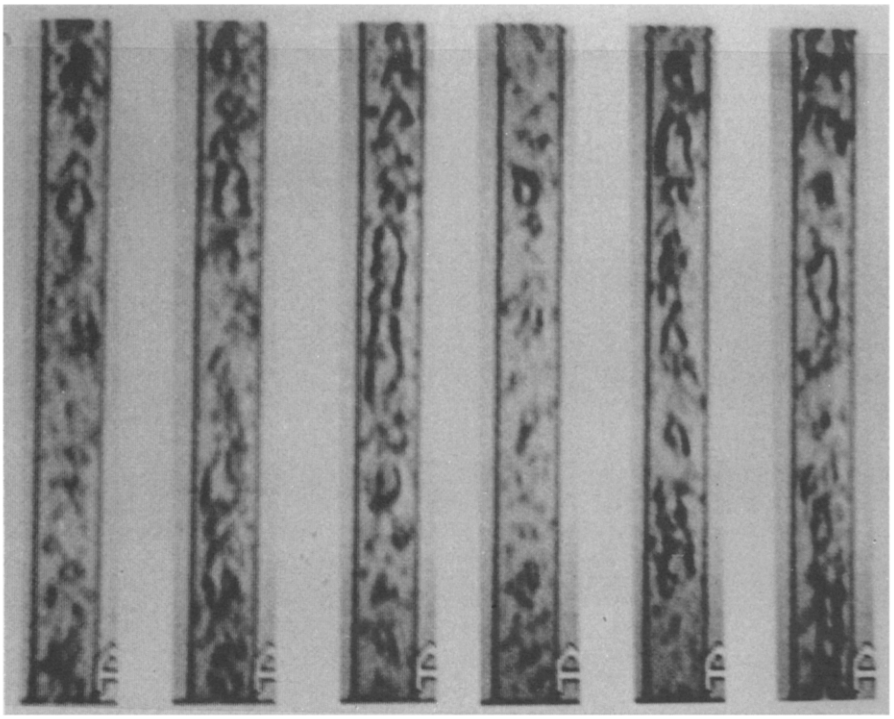

Figure 5. μ-g Flow patterns at $V_{SL} = 2.3$ m/s and $V_{SG} = 0.20$ m/s.

approx. 15.2 MPa, to 689 kPa before it passed to the mass flow controller. The air flow was controlled by a computer through a mass flow controller. The controller has a range of 0–100 SLM (standard liters per minute), and an accuracy of 0.5 SLM. Both the turbine meter and the mass flow controller were calibrated prior to each flight.

Pressure taps of 0.5 mm dia. were spaced 76 cm apart and connected to pressure transducers for absolute and differential pressure-drop measurements. The transducer output for the pressure-drop measurement is a 0–5 V signal, and has a rated accuracy of 0.5% full scale. The absolute pressure transducer is a sealed unit with a range of 0–345 kPa, and an accuracy of 0.5% full scale. The absolute pressure in the test section was in the range 55–83 kPa, and the temperature varied from 35 to 40°C. An accelerometer was used to record the actual g-level. A typical change with respect to time during the flight is given in figure 2. It took about 5 s for the gravity to change from about 1.8 g_0 to μ-g. The μ-g duration lasted aobut 20 s. During the μ-g period, the gravity level may vary within $g/g_0 < 0.03$.

During each parabola, the absolute pressure, pressure difference, liquid and gas flow rates and the g-level were sampled at a rate of 3 points/s. All the data were acquired using an IBM 80286 compatible computer. The computer has a built-in 48-channel programmable gain and a 12-bit data acquisition system. Two-phase flow patterns were recorded on a Hi-8 mm videocamera at a speed of 60 fps. It should be noted that while the frame rate was only 60 fps, the shutter speed was 1/2000 s, thus significantly reducing the blur in the image. The combination of the high shutter speed and the frame-by-frame analysis allowed for a good judgement on the flow patterns.

OBSERVATIONS

Very few data on two-phase gas–liquid flow patterns at μ-g conditions are available in the literature. The method which has been mostly used to describe the flow patterns is the analogy to flow at the normal gravity condition. The flow regime is usually divided into three categories: bubble flow; slug flow; and annular flow. Efforts have been made to model the transition boundaries between the different flow regimes. However, in the absence of gravity (which plays a

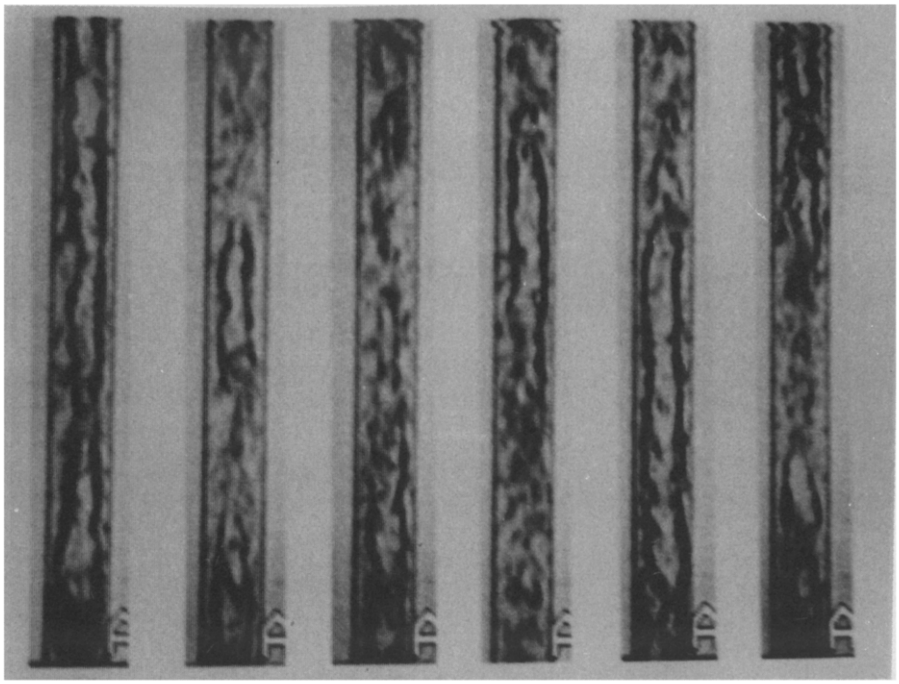

1 2 3 4 5 6

Figure 6. μ-g Flow patterns at $V_{SL} = 2.3$ m/s and $V_{SG} = 0.79$ m/s.

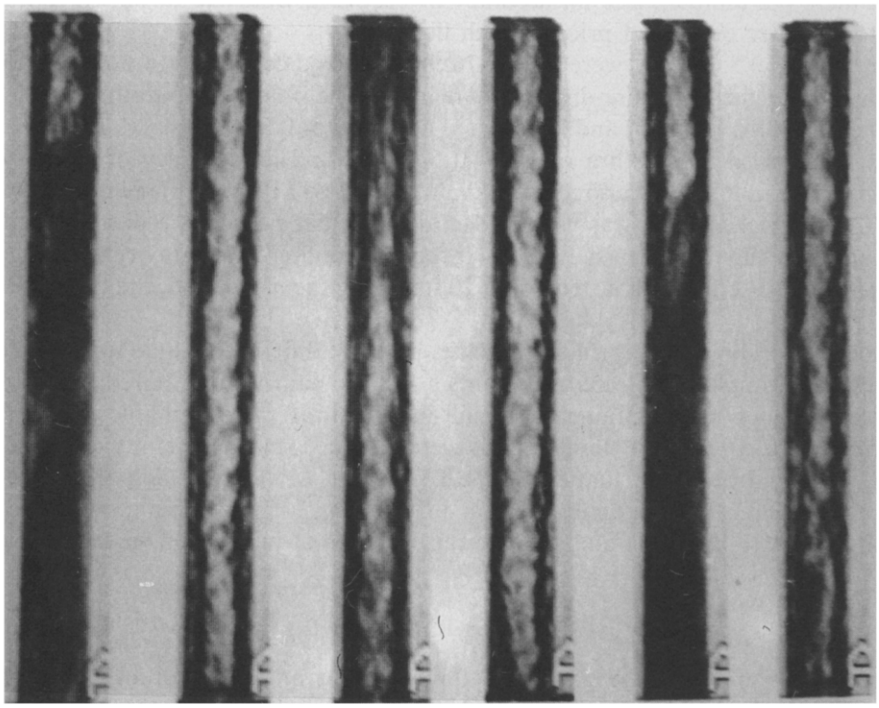

1 2 3 4 5 6

Figure 7. μ-g Flow patterns at $V_{SL} = 2.3$ m/s and $V_{SG} = 3.98$ m/s.

dominant role in the physical process at normal gravity condition), the two-phase flow transitions are governed by a different balance of forces. The method used to describe flow patterns at normal gravity conditions may not be completely appropriate (Rezkallah 1990).

The recorded flow observations were examined on a frame-by-frame basis. Visual observations indicated that the two-phase flow configuration underwent a significant change when the gravity level changed from about 2-g to μ-g conditions. From the image analysis, it appears that in the worst case, it only takes < 3 s for the two-phase mixture to "settle" into the new flow regime. A series of prints of frames at different gas and liquid velocities has been selected to convey the basic flow pattern observations that were present in the vertical upward observation test section. The gravity level in the vertical direction (with respect to the aircraft floor) was sometimes as high as $0.03\,g_0$. At low liquid flow rates, this residual gravity resulted in buoyancy effects that may have influenced the flow patterns.

Figure 3 shows the flow patterns at $V_{SL} = 0.2$ m/s and $V_{SG} = 0.11$ m/s. Hydrodynamically stable, spherically nosed "Taylor" bubbles move along the pipe, separated by liquid slugs which may contain several small gas bubbles (frame 4). Both bubble and slug lengths vary considerably. The length of Taylor bubbles ranges from 5 to 20 times the tube diameter. In some cases (frames 2, 5 and 6), there are very thin membranes in the Taylor bubbles that bridge the gas bubble (or give the appearance of two or more connected bubbles). By observing the relative movement between the tiny gas bubbles in the liquid slug and the Taylor bubbles, it seems that both the Taylor bubble and the liquid slug move at the same speed. The local relative velocity must be very small if it exists at all. At this flow condition, the shape of the bubbles is decided mainly by the surface-tension force, as well as the turbulent force in the liquid. This is perhaps the reason for the spherically nosed Taylor bubbles, and almost spherical small gas bubbles in the liquid slugs (frames 1, 2 and 5). The liquid Reynolds number, Re_{SL}, based on the liquid superficial velocity, is approx. 2000 in this case, which is about the critical value for transition from laminar to turbulent flow in single-phase flow. The disturbances in the liquid phase are responsible for the distortion of the gas bubbles in the liquid slugs.

Flow patterns at $V_{SL} = 0.2$ m/s and $V_{SG} = 6.97$ m/s are given in figure 4. It is found that the liquid slug in the previous flow pattern has been gradually replaced by a frothy slug (frames 3 and 5). The liquid phase has been broken into droplets and mixed with the gas phase, giving it the appearance of a frothy mixture. The liquid droplets continuously deposit onto the liquid film at the wall. As the local thickness of the film increases, the liquid is entrained back into the core flow again. As a result, it seems that the slug of the liquid droplets moves at a speed higher than the liquid film at the wall and lower than the gas phase at the core. Outside the frothy slug region, it is a typical annular flow; gas is flowing at the center core and liquid is flowing as a film at the wall. The transition from slug to annular flow is a slow, gradual process. After a slug flow pattern is formed, and with a further increase in the gas flow rate, the gas in the Taylor bubbles breaks into the liquid slugs forming many small gas bubbles. As the gas flow rate increases further, the density of the gas bubbles increases and eventually the gas bubbles form a continuous gas phase filling what was previously occupied by the liquid slugs. At these flow rates, the gas inertial force is comparable with that due to surface tension. The inertial force gradually overcomes surface tension. Similar phenomena were also reported by Dukler *et al.* (1988) where they described it as a "locally thick" annular film. The frothy slugs become thinner as the gas flow rate increases until eventually a fully annular flow pattern is established.

At a high liquid flow rate and a relatively low gas flow rate, e.g. at $V_{SL} = 2.3$ m/s and $V_{SG} = 0.20$ m/s, a bubble flow (or perhaps a transitional flow from bubble-to-slug) is observed in the tube, as shown in figure 5. The size, shape and length of the gas bubbles vary considerably, but still with a diameter that is smaller than the tube diameter. The shape of the bubbles is quite irregular due to the high turbulence in the liquid phase ($Re_{SL} = 22{,}000$).

At the same liquid superficial velocity ($V_{SL} = 2.3$ m/s), and a higher gas superficial velocity ($V_{SG} = 0.79$ m/s), irregular Taylor shape bubbles are formed in the center of the tube with some fine gas bubbles dispersed in them. These large bubbles are separated by liquid slugs containing some fine bubbles in them as well, as shown in figure 6. At a yet higher gas velocity ($V_{SG} = 3.98$), frothly slug–annular flow occurs. For such high gas concentrations, the frothy liquid portions are more frequent, and also quite packed, as shown in figure 7.

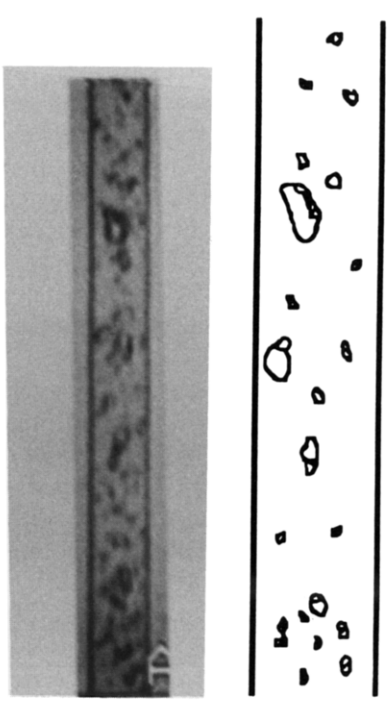

(a) Bubble flow

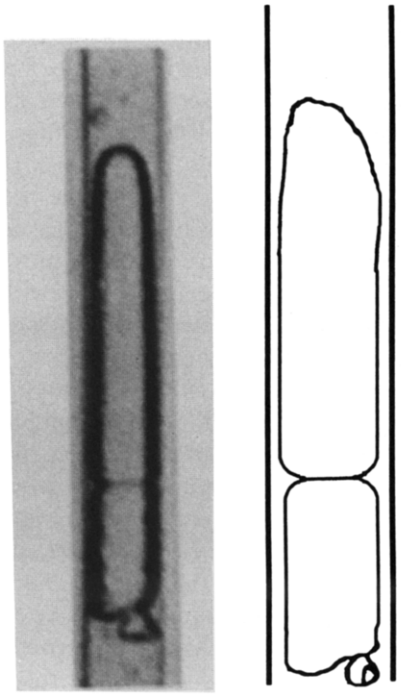

(b) Slug flow

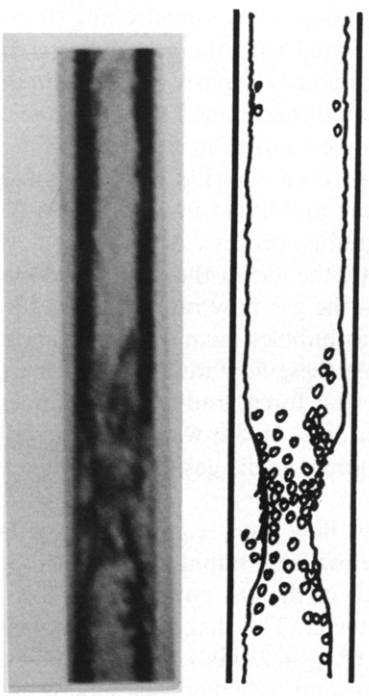

(c) Frothy slug-annular flow

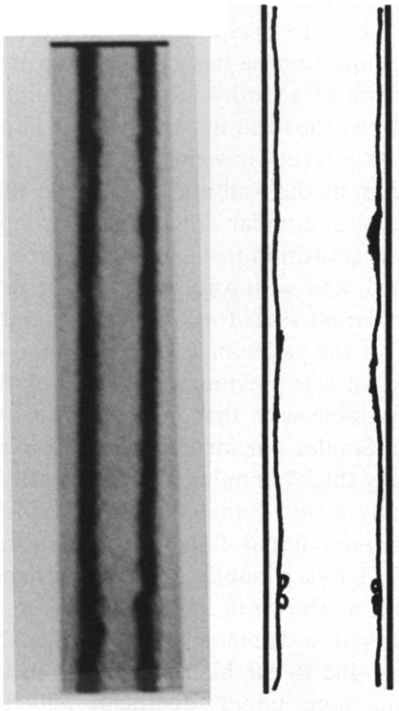

(d) Annular flow

Figure 8. Typical two-phase flow patterns at μ-g conditions.

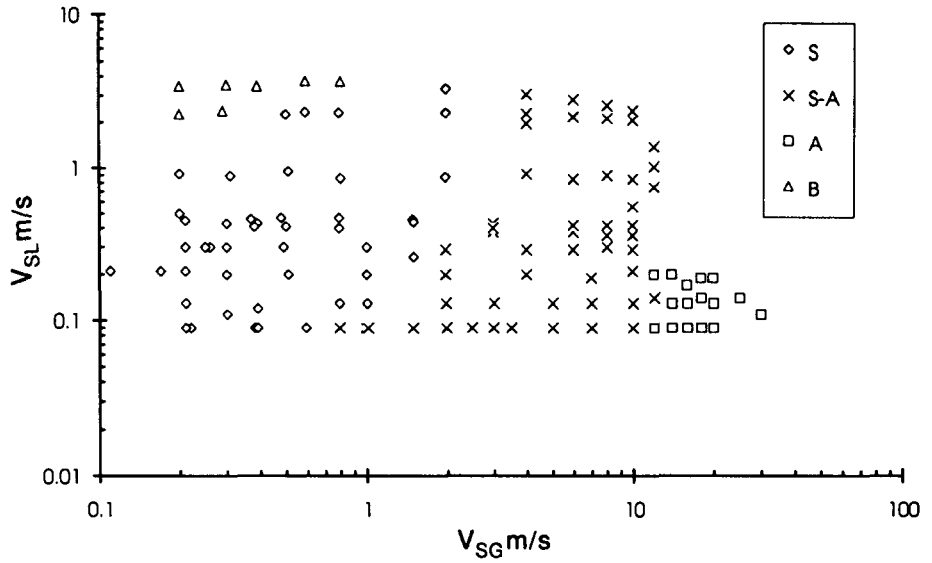

Figure 9. μ-g flow pattern observations.

FLOW PATTERN DEFINITIONS

Basically four flow patterns are observed to exist under μ-g conditions in the range of the liquid and gas flow rates examined in the present study. The first two are what could be described as conventional bubble and slug flows. Bubble flow is recognized when the gas bubbles are a size less than or equal to the tube diameter, such as in figure 8(a). Slug flow [figure 8(b)] is observed when the length of the gas bubbles is greater than the tube diameter, and the diameter of the bubbles is close to the tube diameter. The liquid slugs may or may not contain small gas bubbles. The third type of flow, figure 8(c), is named "frothy slug–annular" flow, in which case the liquid is flowing in the form of a film at the tube wall, and the gas phase is flowing in the center with frequent appearances of frothy slugs in it. Because the details of the frothy slugs cannot be seen clearly, it is speculated that the frothy slugs contain fine gas bubbles in a liquid continuum at relatively low gas flow rates; or tiny liquid droplets in a gas continuum at relatively high gas flow rates. Annular flow [figure 8(d)] is observed when the liquid phase flows at the tube wall and the

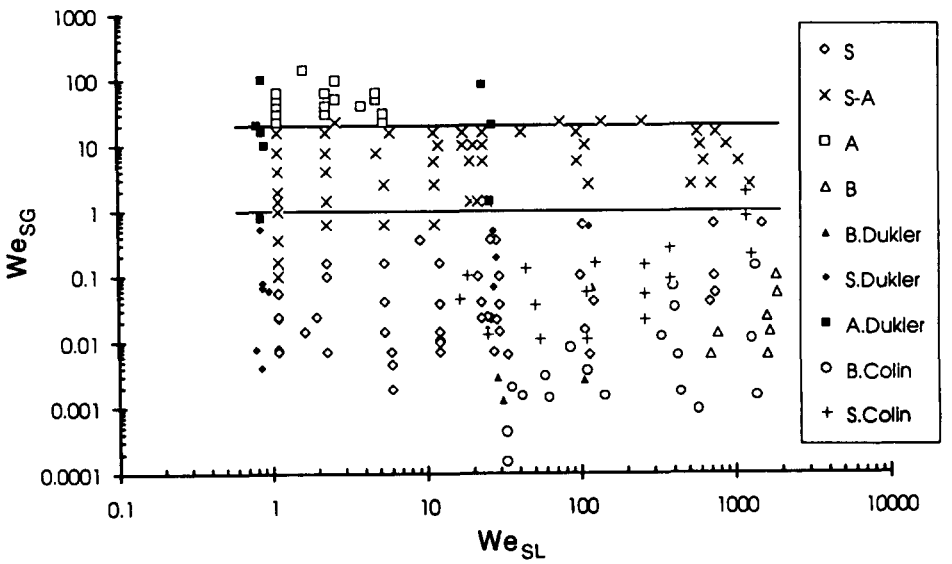

Figure 10. μ-g flow pattern map based on We_{SL} and We_{SG}.

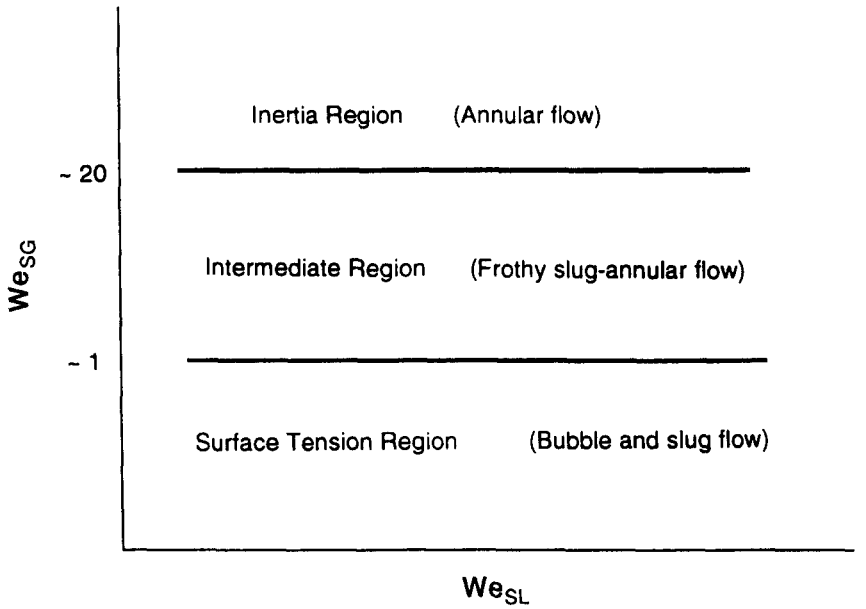

Figure 11. Two-phase flow regions at μ-g conditions.

gas phase flows uninterruptedly at the center of the tube. The gas core may contain dispersed liquid droplets. The flow pattern map according to these definitions is given in figure 9.

FLOW PATTERN TRANSITIONS

Generally speaking, in a two-phase flow, there are several forces acting on the mixture, each of which has some impact on the overall flow configuration. These include the forces due to inertia, buoyancy, surface tension and turbulent eddies. The flow pattern is sometimes determined by a delicate balance of these forces. At low liquid flow rates, forces due to turbulence are negligible compared to other forces. The influence of the buoyancy force due to gravity can be evaluated by the Froude number, Fr, and Eotvos number, Eo. Fr is defined as

$$\mathrm{Fr} = \frac{V_m^2}{gD} = \frac{\text{inertial force}}{\text{buoyancy force}}, \qquad [1]$$

where the velocity V_m is the sum of the gas and liquid superficial velocities V_{SG} and V_{SL}, $V_m = V_{SG} + V_{SL}$, g is the apparent gravity and D is the diameter of the test tube. The average g-level in the present experiment is $0.02\,g_0$. For $V_m = 0.2$, Fr = 21.4; and for $V_m = 0.4$, Fr = 85.6. Thus, inertial forces are much larger than buoyancy forces.

Eo is represented by

$$\mathrm{Eo} = \frac{(\rho_L - \rho_G)gD^2}{\sigma} = \frac{\text{buoyancy force}}{\text{surface tension}}, \qquad [2]$$

where ρ is density and σ is surface tension. The value of Eo is estimated to be 0.25 for the present case. This suggests that the buoyancy force may not be neglected with complete confidence compared to surface tension in the present experiment. Even if the buoyancy force is still playing a role, that role is minor in comparison with other dominant forces under μ-g conditions; namely, those due to inertia and surface tension (especially when the inertial force is large).

The weber number, We, is defined as

$$\mathrm{We} = \frac{V^2 D\rho}{\sigma} = \frac{\text{inertial force}}{\text{surface tension}}, \qquad [3]$$

which represents the balance between the inertial force and surface tension. This dimensionless

group must be an important correlating parameter at μ-g conditions. A flow pattern map based on the We for both phases (We_{SG} vs We_{SL}) is given in figure 10. Also plotted in the same figure are the experimental results from Dukler *et al.* (1988) and Colin *et al.* (1991).

At low gas velocity, and hence for a low We_{SG}, surface tension is dominant. The flow is a bubbly flow and the bubble shape is determined by the surface tension. After the mixer, spherical bubbles of a few millimeters in diameter appear in the tube. The coalescence of small bubbles due to the collision of neighboring ones gives rise to the formation of larger bubbles. The collision rate, in addition to other factors, is a function of void fraction, tube diameter and tube length. The length-to-diameter ratio, L/D, must be an important parameter in determining the bubble size. The length ratio is 50 for the experimental facility of Colin *et al.* (1991) and approx. 63 for that of Dukler *et al.* (1988). In the present study, the ratio is 84. The difference in the developing length in the three cases could perhaps explain the discrepancy in the location of the boundary between bubble and slug flow among these experimental data when that transition boundary is plotted using V_{SL}–V_{SG} coordinates for the map.

Dukler *et al.* (1988) suggested that the transition from bubble to slug flow takes place when $\epsilon = 0.45$, where ϵ is the void fraction in terms of superficial velocities:

$$\epsilon = \frac{V_{SG}}{V_{SG} + V_{SL}}.$$

This gives

$$V_{SL} = 1.22\ V_{SG} \qquad [4]$$

as the transition criterion from bubble to slug flow. Colin *et al.* (1991) proposed the critical void fraction $\epsilon = 0.20$, which corresponds to

$$V_{SL} = 3.2\ V_{SG} \qquad [5]$$

as the transition criterion. A careful study of the present data indicates that the transition from bubble to slug flow occurs when $\epsilon = 0.18$, this gives

$$V_{SL} = 4.56\ V_{SG} \qquad [6]$$

as the transition criterion from bubble to slug flow. Correlation [6] implies that the transition from bubble to slug flow occurs at a lower gas flow rate for a given liquid flow rate when compared with [4] and [5] above. More research work is needed in order to substantiate these methods of correlation for the bubble–slug transition.

When the gas velocity is increased, the inertial force becomes large enough to overcome surface tension. The gas phase breaks through the liquid slug, and forms tiny packed gas bubbles. This is the beginning of the transition from slug flow to annular flow. It was mentioned above that this transition is a slow and a gradual process, and that it occupies a wide range of liquid and gas flow rates. This transition region was also called frothy slug–annular, due to the continuous appearances of frothy mixtures in the liquid slugs which travel at a velocity that is relatively higher than that of the liquid phase at the wall. As shown in figure 10, the transition from slug flow to frothy slug–annular flow appears to take place at

$$We_{SG} = \frac{\rho_G V_{SG}^2 D}{\sigma} \approx 1. \qquad [7]$$

At the lowest liquid flow rate, the transition begins at a lower We_{SG} i.e. at a lower gas flow rate for constant surface tension. This can be also seen in figure 9, where the transition starts at $V_{SG} \approx 3$ m/s for $V_{SL} > 0.3$ m/s; while for $V_{SL} = 0.09$ m/s, the transition starts at $V_{SG} \approx 0.9$ m/s. This could be attributed to the fact that the buoyancy force is playing some role there. As mentioned earlier, the effect of the residual gravity on the aircraft is most noticeable at the lowest liquid flow rates. Hence, in this region, the flow pattern is decided by the balance of inertial force, surface tension and buoyancy forces.

As shown in figure 10, [7] provides an excellent separation for the slug and annular data of Dukler *et al.* (1988). This indicates that $We_{SG} = 1$ represents, in effect, a transition between two different physical processes. The first is when the forces due to surface tension are significantly

higher than those due to inertia ($We_{SG} < 1$), while the second region is where the two forces are comparable ($1 < We_{SG} < 20$). It should be mentioned, however, that the region defined as annular flow by Dukler *et al.* (1988) includes both the frothy slug–annular and annular flows of the present study. This may be partially due to the difference in the definitions of the flow patterns observed, which is somewhat subjective. The data of Colin *et al.* (1991) cover only the bubble and slug flow. These data are in the surface-tension-controlled region, as seen in figure 10.

As the gas flow rate increases further, the density of the liquid droplets in the frothy slugs decreases, the frothy slugs become thinner and thinner until eventually a fully developed annular flow is established. In this region, the flow pattern is dominated by forces due to inertia. As shown in figure 10, it is found that the annular flow occurs at

$$We_{SG} \approx 20, \qquad [8]$$

i.e. when the surface tension force is as low as 5% of the inertial force. Equation [8] presents the criterion for the transition from frothy slug–annular to annular flow.

Thus, in general, two-phase gas–liquid flow under μ-g conditions can be divided into three main flow regions. These are surface-tension-controlled, intermediate and inertial-force-controlled. The surface-tension-controlled region includes bubble and slug flows; while the intermediate region is occupied by transitional flows such as frothy slug–annular flow. Finally, the third region is the inertial-force-controlled region, which is primarily occupied by annular flow. The three flow regions are shown in figure 11.

CONCLUSIONS

Air–water two-phase flow pattern data at μ-g conditions are reported and analyzed in this paper. Four flow patterns are observed to exist, namely: bubble flow; slug flow; frothy slug–annular flow (transitional flow); and annular flow. Among these, only the frothy slug–annular flow has not been observed at normal gravity conditions.

In the absence of gravity, the buoyancy force due to the density difference is negligible. The flow pattern is determined mainly by the balance between the forces due to inertia and surface tension. When surface tension is larger than the inertial force, it is a bubbly flow. When the void fraction based on superficial velocities is smaller than approx. 0.18, bubble flow exists; otherwise it is a slug flow with long Taylor bubbles. When the inertial force is large enough to balance the surface tension, a condition that corresponds to $We_{SG} \approx 1$, the gas phase gradually breaks into the liquid slugs forming tiny packed gas bubbles in them. This corresponds to the onset of the transition from slug to annular flow. A frothy slug–annular flow pattern is formed. As the gas flow rate increases further, the gas bubbles in the liquid slug gradually form a continuous phase with tiny liquid droplets in it. The transition from slug to annular flow covers a wide range of liquid and gas flow rates. Eventually, at $We_{SG} \approx 20$, inertial forces become dominant compared to those due to surface tension, and a fully annular flow is observed in the tube.

The above transition criterion is obtained from water–air experimental data at $We_{SL} > 1$. Experimental verification for other fluid combinations, and for water–air at $We_{SL} < 1$, is needed. For $We_{SL} < 1$, the transition from slug to annular flow may start at a lower We_{SG}, as suggested by the experimental data near $We_{SL} = 1$, owing to the buoyancy force caused by the residual gravity.

Two-phase gas–liquid flow under μ-g conditions can be divided into three main flow regions. These are: the surface-tension-controlled region, which includes bubble and slug flow; the intermediate, which includes the frothy slug–annular flow (transitional flow); and the inertial-force-controlled region, which is mainly occupied by annular flow. The transitions between the different flow regions can be predicted using a criterion in terms of the gas We.

REFERENCES

COLIN, C., FABRE, J. A. & DUKLER, A. E. 1991 Gas–liquid flow at microgravity conditions—I. Dispersed bubble and slug flow. *Int. J. Multiphase Flow* **17**, 533–544.

DUKLER, A. E., FABRE, J. A., MCQUILLEN, J. B. & VERNON, R. 1988 Gas–liquid flow at microgravity conditions: flow pattern and their transitions. *Int. J. Multiphase Flow* **14,** 389–400.

HEPPNER, D. B., KING, C. D. & LITTLES, J. W. 1975 Zero-gravity experiments in two-phase fluids flow patterns. Presented at the *ICES Conf.*, San Francisco, CA, ASME Paper No. TS-ENAS-24.

HUCKERBY, C. S. & REZKALLAH, K. S. 1992a Flow-pattern observations in two-phase gas–liquid flow in a straight tube under normal and microgravity conditions. *AIChE Proc.* **88,** 139–147.

HUCKERBY, C. S. & REZKALLAH, K. S. 1992b Flow-pattern observations in two-phase gas-liquid flow in a straight tube under microgravity conditions. In *Proc. SPACEBOUND '92 Conf.*, Ottawa, Ontario, pp. 68–74.

KARRI, S. B. R. & MATHUR, V. K. 1988 Two-phase flow pattern map predictions under microgravity. *AIChE Jl* **34,** 137–139.

LEE, D., BEST, F. R. & MCGRAW, N. 1987 Microgravity two-phase flow regime modeling. Presented at the *3rd Proc. Nuclear Thermal Hydraulics*, Los Angeles, CA.

REZKALLAH, K. S. 1990 A comparison of existing flow-pattern predictions during forced-convective two-phase flow under microgravity conditions. *Int. J. Multiphase Flow* **16,** 243–259.

REZKALLAH, K. S., HUCKERBY, C. S. & TAO, Y. 1990 Understanding two-phase, liquid–gas behavior at microgravity environment: a force analysis approach. *Proc. CSME Forum* **IV,** 85–90.

TAITEL, Y., BARNEA, D. & DUKLER, A. E. 1980 Modeling flow pattern transitions for steady upward gas–liquid flow in vertical tubes. *AIChE Jl* **26,** 245–354.

TAITEL, Y. & DUKLER, A. E. 1976 A model for predicting flow regime transition in horizontal and near horizontal gas–liquid flow. *AIChE Jl* **22,** 47–55.

WEISMAN, J. & KANG, S. Y. 1981 Flow pattern transitions in vertical and upwardly inclined lines. *Int. J. Multiphase Flow* **7,** 271–291.

WEISMAN, J., DUNCAN, D., GIBSON, J. & CRAWFORD, T. 1979 Effects of fluid properties and pipe diameter on two-phase flow patterns in horizontal lines. *Int. J. Multiphase Flow* **5,** 437–462.